

**Cationic Lipid-DNA Complexes for Gene Therapy:  
Understanding the Relationship between Complex Structure  
and Gene Delivery Pathways at the Molecular Level**

Kai Ewert<sup>(1)</sup>, Nelle L. Slack<sup>(1)</sup>, Ayesha Ahmad<sup>(1)</sup>, Heather M. Evans<sup>(1)</sup>, Alison J. Lin<sup>(1)</sup>,  
Charles E. Samuel<sup>(2)</sup>, and \*Cyrus R. Safinya<sup>(1)</sup>

<sup>(1)</sup> Materials Department, Physics Department, and Biomolecular Science and  
Engineering Program, University of California, Santa Barbara, CA 93106-5121

<sup>(2)</sup> Molecular, Cellular, and Developmental Biology Department, and Biomolecular  
Science and Engineering Program, University of California, Santa Barbara, CA 93106-  
9610

**\*Corresponding author:**

Tel: (805) 893 8635, Fax: (805) 893 7221, e-mail: [safinya@mrl.ucsb.edu](mailto:safinya@mrl.ucsb.edu)

**Key Words:** gene therapy, gene delivery, nonviral, small-angle x-ray scattering,  
multivalent, cationic liposomes, lipofection

## Abbreviations:

BSA	Bovine serum albumin
CL	Cationic liposome
DMEM	Dubellco's modified Eagle's medium.
DMRIE	2,3-Di(myristyloxy)propyl(2-hydroxyethyl)dimethylammonium bromide
DOPC	1,2-Dioleoyl- <i>sn</i> -glycerophosphatidylcholine
DOPE	1,2-Dioleoyl- <i>sn</i> -glycerophosphatidylethanolamine
DOSPA	2,3-Dioleyloxy- <i>N</i> -[2-(spermincarboxamido)ethyl]- <i>N,N</i> -dimethyl-1-propylammonium chloride
DOTAP	2,3-Dioleyloxypropyltrimethylammonium chloride
$H_{II}^c$	Inverted hexagonal phase of lipid-DNA complexes
LSCM	Laser scanning confocal microscopy
$L_{\alpha}^c$	Lamellar phase of lipid-DNA complexes
MVL5	<i>N</i> 1-[2-((1 <i>S</i> )-1-[(3-Aminopropyl)amino]-4-[di(3-aminopropyl)amino]butylcarboxamido)ethyl]-3,4-di[oleylloxy]-benzamide
NLS	Nuclear localization sequence
PEG	Poly(ethylene glycol)
RLU	Relative light units
SAXS	Small angle x-ray scattering
TE	Transfection efficiency
XRD	X-ray diffraction
$\kappa$	Membrane bending rigidity
$\kappa_G$	Membrane Gaussian modulus
$\sigma_M$	Membrane charge density

## ABSTRACT

Cationic liposomes (CLs) are used as gene vectors (carriers) in worldwide human clinical trials of non-viral gene therapy. These lipid-gene complexes have the potential of transferring large pieces of DNA of up to 1 million base-pairs into cells. As our understanding of the mechanisms of action of CL-DNA complexes remains poor, transfection efficiencies are still low compared to gene delivery with viral vectors. We describe recent studies with a combination of techniques (synchrotron x-ray diffraction for structure determination, laser-scanning confocal microscopy to probe the interactions of CL-DNA particles with cells, and luciferase reporter-gene expression assays to measure transfection efficiencies in mammalian cells), which collectively are beginning to unravel the relationship between the distinctly structured CL-DNA complexes and their transfection efficiency. The work described here is applicable to transfection optimization in ex vivo cell transfection, where cells are removed and returned to patients after transfection. CL-DNA complexes primarily form a multilayered sandwich structure with DNA layered between the cationic lipids (labeled  $L_{\alpha}^c$ ). On rare occasions, an inverted hexagonal structure with DNA encapsulated in lipid tubules (labeled  $H_{II}^c$ ) is observed. A major recent insight is that for  $L_{\alpha}^c$  complexes the membrane charge density  $\sigma_M$  of the CL-vector, rather than the charge of the cationic lipid alone, is a key universal parameter that governs the transfection efficiency of  $L_{\alpha}^c$  complexes in cells. The parameter  $\sigma_M$  is a measure of the average charge per unit area of the membrane, thus taking into account the amount of neutral lipids. In contrast to  $L_{\alpha}^c$  complexes,  $H_{II}^c$  complexes containing the lipid 1,2-dioleoyl-*sn*-glycerophosphatidylethanolamine (DOPE) exhibit no dependence on  $\sigma_M$ . The current limiting factor to transfection by cationic lipid

vectors appears to be the tight association of a fraction of the delivered exogenous DNA with cationic cellular molecules, which may prevent optimal transcriptional activity. Future directions are outlined which make use of surface-functionalized CL-DNA complexes suitable for transfection in vivo.

## INTRODUCTION

The field of gene delivery by synthetic (non-viral) vectors continues to attract the interest of a large number of research groups, motivated mainly by the promises of gene therapy [1,2,3,4,5,6,7]. Following initial landmark studies [8,9,10], cationic liposomes (CLs; closed bilayer membrane shells of lipid molecules shown in Fig. (1)) have been established as one of the most prevalent synthetic vectors [2]. They are already used widely for in vitro transfection of mammalian cells in research applications. To enable the use of CL-DNA complexes in gene therapy, their mechanism of action is investigated extensively in many laboratories, concurrently with ongoing, mostly empirical, clinical trials, e.g. to develop cancer vaccines [1,2,3,6]. Most revealing, a current compilation (Table 1) [11] of open gene therapy clinical trials worldwide shows that among 474 trials, over one quarter (126) are with non-viral methods. These are in turn nearly equally split between lipofection-based vectors (including liposomes as well as mixtures of DNA with lipid, polymer, and other small molecules described in the articles in this issue) and naked DNA.

Insert Table 1.

A sense of urgency for developing efficient synthetic carriers stems from the recent tragic events associated with the use of engineered adenovirus vectors. A patient died in a clinical trial due to an unanticipated severe immune response [12]. This points to an important advantage of CL-vectors over viral carriers, namely, the lack of a specific immune response due to the absence of viral peptides and proteins. In addition, in current trials using modified retrovirus vectors to treat children with severe combined

immunodeficiency (SCID), a French gene therapy team faced a major setback when one patient (out of ten) developed a blood disorder similar to leukemia. The disease was confirmed to have resulted from insertion of the transferred DNA into the initial coding region of a gene related to the early development of blood cells [13]. Moreover, while viral capsids have a maximum DNA-carrying capacity of about 40,000 base-pairs [5], CL-DNA complexes place no limit on the size of the DNA, since the vector is formed by self-assembly [14,15,16]. Thus, if complexed with human artificial chromosomes [17,18], optimally designed CL-vectors offer the potential of delivering multiple human genes and regulatory sequences extending over hundreds of thousands of DNA base-pairs. In fact, fractions of an artificial human chromosome with a size of the order of 1 million base-pairs have been transferred into cells using cationic lipids as a vector, albeit extremely inefficiently [17,18].

When solutions of DNA and cationic liposomes are combined, CL-DNA complexes form spontaneously. This is schematically illustrated in Fig. (1). The entropy gain associated with the release of tightly bound counterions from the DNA and the lipid bilayers provides the main driving force for this process. The liposomes are made up of at least two lipids, a cationic lipid and a neutral lipid (sometimes called helper lipid). Depending on the ratio of charges on the cationic lipid and the DNA, anionic, neutral or cationic complexes are obtained. We refer to neutral complexes, where the charges on the DNA exactly match those on the cationic lipids, as isoelectric. For transfection, positively charged complexes are used, as this promotes adhesive interactions with the cell's plasma membrane (see below).

Insert Fig. 1

In spite of all the promise CLs hold as gene vectors, their transfection efficiency (TE), which is a measure of the amount of successfully transferred and expressed DNA, remains low compared to that of viral vectors. This has spurred intense research activity aimed at enhancing TE [1,2,3,4,5,6,7]. Maximizing the transfection efficiencies of non-viral vectors requires a full understanding of the supramolecular structures of CL-DNA complexes, their interactions with cell membranes and the events leading to release of DNA inside the cell for possible expression. Recent synchrotron small angle x-ray diffraction (XRD) work has solved the two types of structures observed in CL-DNA complexes. These are a multilamellar structure with DNA monolayers sandwiched between cationic membranes ( $L_{\alpha}^c$ ) [14], and an inverted hexagonal structure with DNA encapsulated within cationic lipid monolayer tubes ( $H_{II}^c$ ). Both structures are shown in Fig. (2) [15]. We are now beginning to understand the parameters governing assembly and properties of the supramolecular structures of CL-DNA complexes in different lipid-membrane systems [14,15,19,20,21,22]. The transfection efficiencies of nonviral delivery methods may be improved through these insights into transfection-related mechanisms at the molecular and self-assembled levels as we describe below.

Insert Fig. 2

Our work aims at unraveling the mechanisms of transfection by CL-DNA complexes at the molecular to cellular level. In particular, we focus on the influence of the structure of the complex and, within a given structure (lamellar  $L_{\alpha}^c$  or inverted hexagonal  $H_{II}^c$ ), the chemical (e.g. membrane charge density) and physical (e.g.

mechanical properties of the membrane) parameters of the membranes forming the complex. As an example, the mechanical properties of a lipid membrane are determined by its bending rigidity  $\kappa$  and its so-called Gaussian modulus  $\kappa_g$ . The latter characterizes the tendency of a membrane to form pores; thus, CL-DNA complexes with large Gaussian moduli may show enhanced transfection efficiency because of their potential tendency to form energetically favored pores with endosomal membranes releasing DNA into the cytoplasm (see e.g. Fig. (10)).

Our studies are carried out by employing synchrotron XRD for structure determination, reporter gene assays to determine transfection efficiency, and 3-dimensional laser scanning confocal microscopy (LSCM) to image complex pathways and their interactions with cells. The combination of these three characterization methods allows us to interpret the different interactions between high and low transfection efficiency complexes and cells, as observed in confocal microscopy, based on knowledge of the structure of the complexes. The experiments utilize commercially available lipids (cf. Fig. (3)) as well as lipids with multivalent cationic head-groups that were newly synthesized for the purpose of clarifying the precise role of the membrane charge density [23,24].

The *in vitro* studies we describe in this review should apply to TE optimization in *ex vivo* cell transfection, where cells are removed and returned to patients after transfection. In particular, our studies aimed at understanding the key mechanisms underlying TE in continuous (dividing) cell lines should aid clinical efforts to develop efficient CL-vector cancer vaccines in *ex vivo* applications. Those vaccines are intended to induce transient expression of genes coding for immuno-stimulatory proteins in



dividing cells [2,6,10,25,26]. Thus, the nuclear membrane, which dissolves during mitosis, is not considered a barrier to the delivery and expression of DNA.

Insert Fig. 3

In the final “Future Direction” section of this review we outline ongoing experiments in our laboratory using a new class of surface-functionalized CL-DNA complexes, which contain recently synthesized peptide-lipids with specific sequences for targeting of the cell surface and the nucleus [27]. As we describe, such surface-functionalized CL-DNA complexes should be suitable for future in vivo and systemic delivery studies. While the majority of our current effort is focused on optimizing transfection in continuous cell lines, we point out that experiments on non-dividing cells blocked at the G1/S point will be feasible with the surface-functionalized CL-DNA complexes containing peptide-lipids with a nuclear localization sequence (NLS). These experiments will serve as models of transfection in cell lines that either divide very slowly or are non-dividing (e.g. differentiated nerve cells).

## **THE RELATION OF MEMBRANE CHARGE DENSITY AND TRANSFECTION EFFICIENCY OF CATIONIC LIPID-DNA COMPLEXES**

A critical requirement for enhancing the transfection efficiency of synthetic carriers is a full understanding of the different structures of CL-DNA complexes and the physical and chemical basis of their interactions with cellular components. To this end, we examine the structure-dependence of DNA delivery through imaging and transfection studies of CL-DNA complexes that exhibit one of the two known structural phases,  $L_{\alpha}^c$

or  $H_{II}^c$  [14,15]. Three-dimensional LSCM allows direct imaging of complexes and their interactions with cells, and reporter gene transfection studies give a statistically meaningful measure of the total amount of protein synthesized by cells from delivered DNA.

There are many parameters that can be varied to optimize transfection by CL-DNA complexes, e.g. lipid structure, lipid charge, lipid to DNA charge ratio, or the amount of neutral lipid. We are particularly interested in understanding these as factors that influence the properties of the self-assembled system as a whole, enabling a generalized view. One of these properties is the membrane charge density  $\sigma_M$ , defined as the total charge of the membrane due to the cationic lipid headgroups divided by the total area of the membrane. For isoelectric CL-DNA complexes in the  $L_{\alpha}^c$  phase, the average spacing  $d_{DNA}$  between DNA molecules can be expressed in terms of the average distance per anionic charge along the DNA backbone ( $l_0$ ), and the membrane charge density  $\sigma_M$ :  $d_{DNA} = e/(l_0\sigma_M)$  [14,19]. Thus, the DNA interaxial spacing is a measure of  $\sigma_M$  and decreases as the membrane charge density increases. For positively charged complexes,  $\sigma_M$  can no longer be directly calculated from  $d_{DNA}$ , but the same qualitative relationship still holds.

To check whether  $\sigma_M$  is a relevant chemical parameter of CL-DNA complexes relating to TE, we performed experiments in which we varied  $\sigma_M$  systematically for lamellar and inverted hexagonal phases. We investigated the effect on TE and also, via confocal imaging, the pathways of gene delivery into mouse L cells. The structures of the cationic and neutral lipids used in these first studies are given in Fig. (3). The cationic lipids were either commercially available or gifts from other investigators. As

neutral lipids, we used 1,2-dioleoyl-*sn*-glycerophosphatidylethanolamine (DOPE) and 1,2-dioleoyl-*sn*-glycerophosphatidylcholine (DOPC). DOPE is one of the main neutral lipids currently in use in gene therapy applications of CLs. To fully explore the validity of our findings, further experiments using new, recently synthesized lipids with multivalent cationic head groups were performed [23,24].

Prior to our studies, TE measurements by other groups had shown that in mixtures of the monovalent cationic lipid 2,3-dioleoyloxypropyltrimethylammonium chloride (DOTAP) and neutral lipids, typically at a weight ratio between 1:1 and 1:3, DOPE aided whereas DOPC severely suppressed transfection [28,29]. Therefore, it seemed that DOPE-based  $H_{II}^C$  complexes always transfect more efficiently than  $L_{\alpha}^C$  complexes. Our findings show that the difference in performance between the two types of complexes is subtler than previously believed and that there are regimes of composition where the TE of complexes in the  $L_{\alpha}^C$  phase becomes as high as that of the best  $H_{II}^C$  complexes.

Insert Fig. 4

In our first set of experiments, the lipid mixtures for  $L_{\alpha}^C$  complexes (Fig. (4), left) were comprised of monovalent cationic DOTAP mixed with neutral DOPC. Those for  $H_{II}^C$  complexes (Fig. (4), right) contained DOTAP mixed with neutral DOPE. We used positively charged CL-DNA complexes prepared at  $\rho = \text{DOTAP/DNA (wt./wt.)} = 6$  with supercoiled pGL3 (luciferase gene/SV 40 promoter; from Promega Corp.) plasmid DNA. The isoelectric point, where the charges of the DNA are exactly neutralized by those of the lipid, is at  $\rho = 2.2$ . We chose the weight ratio  $\rho = 6$ , equivalent to a cationic to

anionic charge ratio of 2.8, because it corresponds to the middle of a typical plateau region that is observed when plotting TE as a function of increasing  $\rho$  above the isoelectric point. XRD measurements elucidated the structures of these complexes in water and in Dulbecco's Modified Eagle Medium (DMEM), a common environment for in vitro studies of cells [24,38,30]. Synchrotron small angle x-ray scattering (SAXS) patterns of DOTAP/DOPC complexes at the mole fraction  $\Phi_{\text{DOPC}} = 0.67$  (Fig. (4), left) showed sharp peaks at  $q_{001} = 0.083 \text{ \AA}^{-1}$ ,  $q_{002} = 0.166 \text{ \AA}^{-1}$ , with a shoulder peak at  $q_{003} = 0.243 \text{ \AA}^{-1}$  and  $q_{004} = 0.335 \text{ \AA}^{-1}$ , resulting from the layered structure of the  $L_{\alpha}^{\text{C}}$  phase. The interlayer spacing is  $d = \delta_{\text{m}} + \delta_{\text{w}} = 2\pi/q_{001} = 75.70 \text{ \AA}$ , with DNA intercalated between cationic lipid bilayers (cf. Fig. (2)). For DOTAP/DOPE complexes at  $\Phi_{\text{DOPE}} = 0.69$ , SAXS (Fig. (4), right) revealed four orders of Bragg peaks at  $q_{10} = 0.103 \text{ \AA}^{-1}$ ,  $q_{11} = 0.178 \text{ \AA}^{-1}$ ,  $q_{20} = 0.205 \text{ \AA}^{-1}$  and  $q_{21} = 0.270 \text{ \AA}^{-1}$ , denoting the  $H_{\text{II}}^{\text{C}}$  phase with a unit cell spacing  $a = 4\pi/[(3)^{1/2}q_{10}] = 70.44 \text{ \AA}$  (Fig. (4), right, inset and Fig. (2)). Mouse L cells were transfected with CL-DNA complexes using pGL3 DNA that contains the firefly luciferase reporter gene. The TE was measured via the standard luminescence assay as relative light units (RLU) per mg of cell protein [38,30]. The results of these experiments are shown in Fig. (4) (middle), demonstrating that the TE attainable with complexes in the  $H_{\text{II}}^{\text{C}}$  phase at  $\Phi_{\text{DOPE}} = 0.69$  is by more than two decades higher than that of  $L_{\alpha}^{\text{C}}$  complexes at  $\Phi_{\text{DOPC}} = 0.67$ .

Insert Fig. 5

To further understand the structure-function correlation, we examined the transfer process of CL-DNA complexes into cells and the mechanism of the subsequent DNA release using LSCM, which provides an optical resolution of  $\sim 0.3 \mu\text{m}$  in the x and y, and  $\sim 3/4 \mu\text{m}$  in the z direction. By comparing images of the x-y, y-z, and x-z planes, it is possible to determine the position of an object relative to a cell. The complexes were doubly tagged with fluorescent labels, Texas Red-DOPE for lipid and a covalently attached green label for DNA (Mirus Label IT<sup>TM</sup>) [38]. The intensity of the fluorescence sets the detection limit for DNA and lipid, which does not reach the single molecule level for uncondensed DNA. Fig. (5) shows LSCM micrographs of mouse L cells taken six hours after the addition of complexes. In Fig. (5 (A)), a typical image of a cell transfected with  $H_{II}^C$  complexes at  $\Phi_{\text{DOPE}} = 0.69$  is displayed. The lipid fluorescence clearly outlines the plasma membrane, indicating either spontaneous transfer of labeled lipid or fusion of lipid with the plasma membrane (which may have occurred before or after entry through the endocytic pathway [31]). An aggregate of complexes (yellow) is visible inside the cell as well as lipid-free DNA (green) in the cytoplasm. The image shows that the interaction between  $H_{II}^C$  complexes and cells leads to the dissociation and release of DNA from the CL-vector, consistent with the measured high TE.

The corresponding confocal images for  $L_{\alpha}^C$  complexes at  $\Phi_{\text{DOPC}} = 0.67$  are shown in Fig. (5 (B)). In striking contrast to  $H_{II}^C$  complexes, we observed no free DNA. Rather, many individual intact CL-DNA complexes are found inside of the cells. A typical complex is highlighted in Fig. (5 (B)). These results show that at  $\Phi_{\text{DOPC}} = 0.67$ , most of the DNA remains trapped by the CL-vector, consistent with the measured low TE. As there is no fluorescent lipid observed in the cell membrane, fusion is ruled out as a mechanism of cell entry. Thus, the complexes most likely entered the cells through

endocytosis, as also observed by others [31,32,33]. Furthermore, transfection experiments performed in the presence of chloroquine showed that the intact CL-DNA complexes were mostly trapped within endosomes as we will discuss later.

Insert Fig. 6

In further experiments, we observed an unexpected enhancement of the TE by two decades as the concentration of DOPC in  $L_{\alpha}^C$  CL-DNA complexes was reduced. In Fig. (6 (A)) (diamonds), the non-trivial dependence of TE on  $\Phi_{\text{DOPC}}$  for DOPC/DOTAP-DNA complexes is plotted. The transfection efficiency starts low for  $0.5 < \Phi_{\text{DOPC}} < 0.7$  and increases dramatically to a value, at  $\Phi_{\text{DOPC}} = 0.2$ , which rivals that achieved by the DOPE/DOTAP-DNA  $H_{II}^C$  complexes. Similar results were obtained for another univalent cationic lipid 2,3-di(myristyloxy)propyl(2-hydroxyethyl)dimethylammonium bromide (DMRIE) (Fig. (6 (A)), triangles). The key experiment, which led to a deeper understanding of the observed TEs, was a study done with the multivalent cationic lipid 2,3-Dioleyloxy-*N*-[2-(sperminecarboxamido)ethyl]-*N,N*-dimethyl-1-propylammonium chloride (DOSPA) (Fig. (6 (A)), squares) replacing DOTAP. A qualitatively similar trend was observed, with TE decreasing rapidly above a critical  $\Phi_{\text{DOPC}}^*$ . However,  $\Phi_{\text{DOPC}}^*$  was shifted from  $\sim 0.2$ , as observed for DOTAP and DMRIE complexes, to  $0.7 \pm 0.1$  for DOSPA. The main difference between the cationic lipids is their headgroups (Fig. (6), inset). The headgroup of DOSPA has a high charge of up to +5 at a size that is only somewhat larger than that of the DOTAP headgroup. Thus, the charge density (charge per unit area) of the headgroup is much higher for DOSPA and, at a given  $\Phi_{\text{DOPC}}$ , the

membrane charge density  $\sigma_M$  in complexes containing DOSPA also is significantly larger compared to complexes prepared from DOTAP or DMRIE.

In Fig. (6 (B)), the same TE data as in Fig. (6 (A)) is shown, now plotted versus the average membrane charge density  $\sigma_M$ :

$$\sigma_M = eZN_{cl}/(N_{nl}A_{nl} + N_{cl}A_{cl}) = [1 - \Phi_{nl}/(\Phi_{nl} + r\Phi_{cl})]\sigma_{cl} \quad (1)$$

In equation (1) we have defined  $r = A_{cl}/A_{nl}$  as the ratio of the head-group area of the cationic to neutral lipid,  $\sigma_{cl} = eZ/A_{cl}$  as the charge density of the cationic lipid with valence  $Z$ , and  $\Phi_{nl} = N_{nl}/(N_{nl} + N_{cl})$  and  $\Phi_{cl} = N_{cl}/(N_{nl} + N_{cl})$  as the mole fractions of the neutral and cationic lipids, respectively. For the plots in Fig. (6 (B)), we used  $A_{nl} = 72 \text{ \AA}^2$  [34],  $r_{\text{DOTAP}} = r_{\text{DMRIE}} = 1$ ,  $r_{\text{DOSPA}} = 2$ ,  $Z_{\text{DOTAP}} = Z_{\text{DMRIE}} = 1$ ,  $Z_{\text{DOSPA}} = 4$  (expected for  $\text{pH} \approx 7$ ). Since we were unable to obtain well-defined values for the head group area of cationic lipids using standard methods,  $r$  is an adjustable parameter. The values used in the plots agree well with chemical intuition (cf. also inset in Fig. (6)). All other parameters are fixed by the experiment or the chemical structure. Given the complexity of the CL-DNA-cell system, it is remarkable that the data, spread-out when plotted as a function of  $\Phi_{nl}$  (Fig. (6 (A))), coalesce into a single, ‘‘universal’’ curve as a function of  $\sigma_M$ , with TE varying exponentially over nearly four decades as  $\sigma_M$  increases by a factor of  $\approx 8$  (Fig. (6 (B)),  $\sigma_M$  between  $0.0015 \text{ e/\AA}^2$  and  $0.012 \text{ e/\AA}^2$ ). This clearly implies that  $\sigma_M$  is a key universal parameter for transfection with lamellar  $L_\alpha^c$  CL-vectors. We now observe a single optimal  $\sigma_M^* \approx 0.0104 \pm 0.0017 \text{ e/\AA}^2 \approx \text{e}/(100 \text{ \AA}^2)$  (Fig. (6 (B)), arrow) beyond which ( $\sigma_M > \sigma_M^*$ ) the universal TE curve saturates for both univalent and multivalent

cationic lipid containing CL-vectors. The membrane charge density  $\sigma_M$  controls the average DNA interaxial spacing  $d_{\text{DNA}}$  (cf. Fig. (2)) [14,19], which was found to decrease as  $\sigma_M$  increases and level off for  $\sigma_M > \sigma_M^*$  [38]. It is important to note that all TE measurements were done with 2  $\mu\text{g}$  of plasmid DNA at a constant cationic to anionic charge ratio of 2.8 (see above). Thus, every TE data point used the same amount of total charged species (anionic charge from DNA, cationic charge from cationic lipid) and only the membrane charge density of CL-DNA complexes ( $\sigma_M$ ) was varied by adjusting the amount of neutral lipid.

Insert Fig. 7

The TE data show vastly diverse behaviors of  $L_\alpha^c$  CL-DNA complexes between low and high  $\sigma_M$ . As discussed earlier, for low  $\sigma_M = e/(200 \text{ \AA}^2)$ , corresponding to low TE, confocal images show DNA locked within complexes after endocytosis (Fig. (5 (B))). To test the idea that the complexes are trapped in the endosome, we carried out transfection experiments in the presence of chloroquine. This is a well-established bioassay known to enhance the release of material trapped within endosomes [35] by osmotically bursting late-stage endosomes. The endocytic pathway involves lowering the pH inside the endosome and fusion of the endosome with nuclease containing lysosomes, leading to late-stage endosomes. This limits the time available for CL-DNA complexes to escape. Chloroquine is a weak organic base, which can penetrate lipid membranes in the non-protonated state. Once protonated, it can no longer diffuse through the membrane and therefore effectively acts as a buffer selective for acidic cell



compartments. As more and more protons are pumped into the buffered endosome to lower the pH, counterions follow, which eventually causes rupture of the vesicle due to the increased osmotic pressure [36]. The fractional increase ( $TE_{\text{chloroquine}}/TE$ ; note the logarithmic scale) for the DOSPA/DOPC and DOTAP/DOPC systems with added chloroquine, plotted as a function of  $\sigma_M$  (Fig. (7)), shows a large increase by as much as a factor of 60 as  $\sigma_M$  decreases. This indicates that at low  $\sigma_M$ , lamellar  $L_\alpha^c$  complexes are trapped within endosomes, consistent both with the confocal images (Fig. (5 (B))) and the measured low TE without chloroquine. At high  $\sigma_M$ , chloroquine has a much smaller effect on TE with the fractional increase of order unity, implying that endosomal entrapment is not a significant limiting factor.

A comparison of TE as a function of  $\sigma_M$  for DOTAP/DOPC-DNA and DOTAP/DOPE-DNA complexes is shown in Fig. (8). The DOTAP/DOPE system goes through 2 phase transitions:  $L_\alpha^c$  (filled squares) to coexisting  $L_\alpha^c + H_{II}^c$  (squares with cross) to  $H_{II}^c$  (open squares). At high  $\Phi_{\text{DOPE}} > 0.56$ , DOTAP/DOPE-DNA complexes are in the  $H_{II}^c$  phase (open squares) and exhibit high TE. In contrast to DOPC containing complexes, which show a strong dependence on the mole fraction of neutral lipid and therefore  $\sigma_M$ , the TE of DOPE-containing complexes is independent of  $\sigma_M$ . In contrast, high TE requires  $\sigma_M > \sigma_M^*$  for  $L_\alpha^c$  complexes. We can thus conclude from the data that  $\sigma_M$  is an essential parameter for transfection with  $L_\alpha^c$  complexes but not  $H_{II}^c$  complexes. The mechanism of transfection by DOPE containing  $H_{II}^c$  complexes is dominated by other effects as we describe below.

Insert Fig. 8

LSCM images of cells transfected with  $L_{\alpha}^c$  complexes at high  $\sigma_M$  displayed a path of complex uptake and DNA release distinct from both  $L_{\alpha}^c$  complexes at low  $\sigma_M$  (Fig. (5 (B))) and  $H_{II}^c$  complexes (Fig. (5 (A))). A typical confocal image of a cell incubated for 6 h with  $L_{\alpha}^c$  complexes at  $\Phi_{DOPC} = 0.18$  ( $\sigma_M \approx 0.012 \text{ e}/\text{\AA}^2$ ) is shown in Fig. (9). A few intact complexes are visible inside the cell: Fig. (9) (label 2; box 2) shows the equal green (DNA) and red (lipid) fluorescence intensity along the dotted line in the inset. More interestingly, a mass of exogenous DNA successfully transferred into the cytoplasm was also clearly evident (Fig. (9), label 1; box 1 shows the much larger green (DNA) fluorescence intensity along the x-y diagonal). Since there is no indication of transfer of fluorescent lipid to the plasma membrane, the complexes with high  $\sigma_M$  must have entered the cells through endocytosis. The integrated fluorescence intensity of the observed DNA (Fig. (9), box 1) is comparable to that of DNA complexed with lipids (Fig. (9), box 2), indicating that the released DNA is in the form of aggregates. As endosomes contain no known DNA-condensing agent, these aggregates must reside in the cytoplasm, which contains many multivalent cationic biomolecules (e.g. spermine and histones, which become available during the cell cycle) that are able to condense DNA [37]. The presence of lipid-released DNA in the cytoplasm after endocytic uptake of complexes is in agreement with the measured high TE and, moreover, implies fusion between CL-DNA lipids and endosomal membranes, enabling escape from the endosome. This is consistent with our finding that chloroquine has a small effect on TE at high  $\sigma_M$ , suggesting that endosomal escape is not a major obstacle. The confocal image also shows a large aggregate of complexes in on part of the cell (Fig. (9), label 3).

Again, there is no transfer of fluorescent lipid to the cell membrane, which rules out entry by fusion with the plasma membrane. Comparing the changes in fluorescence intensity along the x-y-diagonal (Fig. (9), box 3) and z-axis (Fig. (9), box 4), from the outside toward the inside of the cell, we see an aggregate of complexes caught in the process of dissociation after endocytosis, with released DNA toward the inside of the cell.

Insert Fig. 9

In summary, our 3-dimensional LSCM studies have revealed distinct interactions between CL-DNA complexes and mouse L cells, both for lamellar  $L_{\alpha}^c$  and inverted hexagonal  $H_{II}^c$  nanostructures. Confocal images of  $L_{\alpha}^c$  complexes in cells identified two regimes [38]. For low  $\sigma_M$ , DNA remained trapped in CL-vectors. By contrast, for high  $\sigma_M$ , released DNA was observed in the cytoplasm, indicative of escape from endosomes through fusion. TE studies using the firefly luciferase reporter gene revealed a truly unexpected result: at a constant cationic to anionic charge ratio, TE data for univalent and multivalent cationic lipids merged into a single curve as a function of  $\sigma_M$ , identifying it as a key *universal* parameter [38]. The universal TE curve revealed an optimal membrane charge density ( $\sigma_M^*$ ) where  $L_{\alpha}^c$  complexes with  $\sigma_M > \sigma_M^*$  achieve TEs comparable to that of highly transfecting  $H_{II}^c$  complexes. In contrast to  $H_{II}^c$  complexes, where TE is independent of  $\sigma_M$ , the universal TE curve for  $L_{\alpha}^c$  complexes was found to increase *exponentially* over nearly four decades with increasing  $\sigma_M < \sigma_M^*$ .

**A model of cell entry by  $L_{\alpha}^c$  CL vectors: Dependence on  $\sigma_M$  and elastic moduli of cationic membranes of CL-DNA complexes.** The combined x-ray diffraction, LSCM, and TE data lead to a model of cellular entry via  $L_{\alpha}^c$  CL carriers (Fig. (10)). Previous work indicates that the electrostatic attraction between cationic CL-DNA complexes and mammalian cells is mediated by negatively charged cell surface sulfated proteoglycans (Fig. (10), label a) [39]. Our LSCM images show no evidence of fusion with the plasma membrane, implying that  $L_{\alpha}^c$  complexes enter cells via the endocytic pathway (Fig. (10), labels b and c). This is consistent with results of other research groups and our transfection experiments in the presence of chloroquine. Once inside the cell,  $L_{\alpha}^c$  CL-DNA particles exhibit two distinct types of behavior as revealed by confocal microscopy. At low  $\sigma_M$ , mostly intact  $L_{\alpha}^c$  complexes are observed inside of the cells and TE experiments in the presence of chloroquine are consistent with intact complexes trapped in endosomes (Fig. (10), label c). At high  $\sigma_M$ , LSCM revealed lipid-free DNA inside cells. Since the observed DNA is in a condensed state, it must reside in the cytoplasm (Fig. (10), label e) because of the lack of condensing molecules in the endosome [37]. This observation is consistent with TE data at high  $\sigma_M$ , where the addition of chloroquine does not increase TE.

Insert Fig. 10

From all our data, we conclude that in the regime where transfection efficiency scales exponentially with  $\sigma_M$ , the limiting step in the transfection process is escape from the endosome after endocytosis. The most probable mechanism for this is through fusion

with the endosomal membrane (Fig. (10), label d). The model we propose connects this process with the membrane charge density  $\sigma_M$  of enclosed complexes. For  $\sigma_M < \sigma_M^*$ , the universal TE curve (Fig. (6 (B))) shows TE increasing exponentially as a function of  $\sigma_M$  and therefore suggests a simple model of activated fusion (showing Arrhenius behavior) of complexes with endosomal vesicles. Since fusion is the rate limiting process, TE is proportional to the rate of fusion:

$$\text{Transfection Efficiency} \propto \text{rate of fusion} = \tau^{-1} [\exp(-\delta E/k_B T)], \quad (2)$$

with  $\delta E = \text{energy barrier height} = a \cdot \kappa - b \cdot \sigma_M$ . Here,  $a, b > 0$  are constants and  $\tau^{-1}$  is the collision rate between the trapped CL-DNA particle and the endosomal wall (Fig. (10), label c). The membrane bending modulus  $\kappa$  is a measure of the flexibility of the membrane [40,41,42]. The larger  $\kappa$ , the higher the energy cost associated with bending the membrane. Bending is inevitable in the fusion of membranes, as shown schematically by the arrows in the expanded view of Fig. (10), label d. The energy required for this, which is proportional to  $\kappa$ , thus provides the main barrier to fusion. On the other hand, electrostatic attraction favors membrane adhesion because the fusing membranes are oppositely charged. This results in a lower energy barrier as  $\sigma_M$  increases (Fig. (10), label c, arrows in expanded view), corresponding to the term “ $- b \cdot \sigma_M$ ” in equation (2). The fact that higher  $\sigma_M$  lowers the barrier height and thus appears in the exponent in equation (2) is responsible for the exponential increase of TE observed in our experiments (Fig. (6 (B))). In agreement with our model, a recent theoretical study, which considers fusion between two neutral lipid bilayers (i.e. forming pores between

neighboring membranes), has found that the main energy barrier against fusion is proportional to  $\kappa$  [43]. The same study also implies that the membrane Gaussian modulus  $\kappa_G$  should enhance fusion when  $\kappa_G > 0$ , favoring pore formation. Current work in our group, e.g. with lipids showing a preference for cubic phases (with  $\kappa_G > 0$ ), is aimed at experimentally testing the influence of  $\kappa_G$  and  $\kappa$  on TE.

**A model of cell entry by CL-vectors with the  $H_{II}^C$  structure: Relevance of the outermost lipid layer.** A striking difference between transfection by  $H_{II}^C$  versus  $L_{\alpha}^C$  complexes is that for the former, transfection efficiency is independent of the membrane charge density  $\sigma_M$  (Fig. (8)). Thus, a different mechanism, which is independent of  $\sigma_M$ , must dominate the interaction between  $H_{II}^C$  complexes and cells. The lipid fluorescence, which outlines the plasma membrane in the LSCM images shown in Fig. (5 (A)), indicates mixing of lipids of  $H_{II}^C$  complexes with the plasma membrane, which may have occurred before or after entry through the endocytic pathway. The image shows that the interaction between  $H_{II}^C$  complexes and cells leads to dissociation and release of DNA from the CL-vector consistent with the measured high TE. A mechanism that may be responsible for rapid fusion is shown schematically in Fig. (11). In the top part, a  $H_{II}^C$  complex is shown approaching either the plasma or the endosomal membrane. The cell-surface proteoglycans, which again mediate the attraction between the complex and the membrane (cf. Fig. (10)), have been omitted for the sake of clarity. For lipids forming  $H_{II}^C$  complexes, the preferred membrane curvature is negative, as opposed to  $\approx 0$  for lipids that form the  $L_{\alpha}^C$  structure. Negative curvature is realized for the lipids coating DNA inside the  $H_{II}^C$  complex, but the curvature of the outermost lipid monolayer, which

must cover the  $H_{II}^C$  complex to provide a hydrophilic surface, is positive. This elastically frustrated state of the outer monolayer, which is independent of  $\sigma_M$ , drives the rapid fusion with the plasma or endosomal membrane, leading to release of a layer of DNA and a smaller  $H_{II}^C$  complex as shown in the bottom part of the Fig. (11). In the language of our model for cell entry of  $L_{\alpha}^C$  complexes, the activation energy for fusion of  $H_{II}^C$  complexes with the endosomal membrane is negligible and this step no longer limiting. The outer layer of the released, smaller  $H_{II}^C$  complex is again elastically frustrated and will drive quick release of the remaining DNA through interactions with other membranes, negatively charged cellular proteins or DNA-condensing molecules. By comparison, the bilayers of lamellar  $L_{\alpha}^C$  complexes are inherently more stable. After escaping the endosome through fusion (see Fig. (10), label d), the onion-like (lipid-bilayer/DNA-monolayer) complex is expected to peel much more slowly, *layer-by-layer*, through interactions of the cationic membranes with anionic components of the cell, such as the predominantly anionic cytoskeletal filaments [44], or DNA-condensing biomolecules.

Insert Fig. 11

**Structures and transfection properties of new, ornithine-based multivalent cationic lipids.** To further investigate our finding of a well-defined relationship between transfection efficiency and membrane charge density  $\sigma_M$  in lamellar  $L_{\alpha}^C$  complexes, and to explore more broadly the relevance of  $\sigma_M$  as a key chemical parameter, we have recently synthesized new lipids with multivalent cationic head groups, which we describe

in this section. The general structure of the lipids is shown in Fig. (12), and the lipid head groups are compiled in Table 2. The headgroups are based on the amino acid ornithine, whose structure is shown in Table 2 in the top-left box. A key point is that their charge was varied systematically from +2 (MVL2) to +5 (MVL5). This was achieved by the addition of propyl-amine groups to the original ornithine via Michael addition of acrylonitrile and subsequent hydrogenation [24]. A monovalent lipid (MVL1), based on glycine, was also prepared for comparison.

Insert Fig. 12

Insert Table 2.

Work on one of the new multivalent cationic lipids (MVL5) shows structurally stable complexes with improved transfection efficiency behavior [24]. Optical micrographs of these CL-DNA complexes are shown in Fig. (13), imaged in differential-interference-contrast (left), DNA fluorescence (middle) and lipid fluorescence mode (right). The complexes were prepared using DOPC/MVL5 lipid mixtures which contained 40 wt.-% MVL5 at a cationic lipid to DNA charge ratio of 2.8, which gives optimal transfection for complexes made from DOTAP and DOPC [38]. The observation of co-localization of lipid and DNA by fluorescence microscopy proves the formation of complexes.

Insert Fig. 13



The structure of the CL-DNA complexes was investigated by XRD. In Fig. (14), SAXS patterns are shown for complexes at weight fractions of cationic lipid of 40% (MVL5) and 30% (DOTAP), corresponding to equivalent molar fractions of 31% and 33% of cationic lipid in the membrane. At this composition, the transfection efficiency of the MVL5 complexes is approximately 100-fold higher than that of the DOTAP complexes. The lipid to DNA charge ratio for all complexes was again 2.8. Both CL-DNA complexes are in the lamellar  $L_{\alpha}^c$  phase. As with DOTAP, the  $L_{\alpha}^c$  phase is observed throughout the lipid composition range for MVL5/DOPC/DNA complexes. For the MVL5 complexes in Fig. (14), three peaks at  $q = 0.088 \text{ \AA}^{-1}$ ,  $0.175 \text{ \AA}^{-1}$  and  $0.261 \text{ \AA}^{-1}$  are observed, corresponding to the (00h) peaks of the layered structure with an interlayer spacing  $\delta = 2\pi/q_{001}$  of  $71.2 \text{ \AA}$ .

Insert Fig. 14

The broad peak at  $q_{\text{DNA}} = 0.201 \text{ \AA}^{-1}$  arises from correlations between DNA chains within a water gap and gives their interaxial spacing  $d_{\text{DNA}} = 2\pi/q_{\text{DNA}} = 31.2 \text{ \AA}$  [14,15]. This spacing increases ( $q_{\text{DNA}} = 0.106 \text{ \AA}^{-1}$ , i.e.  $d_{\text{DNA}} = 59.5 \text{ \AA}$ ) for the complexes prepared with an equivalent molar ratio of the univalent lipid DOTAP, reflecting the lower membrane charge density in DOTAP/DOPC complexes due to the smaller head group charge.

Insert Fig. 15

For transfection studies, we compared CL-DNA complexes prepared with DOTAP and MVL5. While the ratio of neutral to cationic lipid was varied, all complexes again had the lipid to DNA charge ratio of 2.8 optimized for the DOTAP/DOPC system. By assigning a charge of +4 to it, incomplete protonation of the MVL5 head group at neutral pH [45] was taken into account. Transfection experiments using mouse fibroblast L-cells and a luciferase reporter assay are displayed in Fig. (15). The new lipid MVL5 gives higher transfection efficiencies for all ratios of neutral to cationic lipid. However, the difference in transfection efficiencies increases dramatically from one to three orders of magnitude as the amount of cationic lipid is reduced from 50 to 20 mol-percent. For MVL5, the transfection efficiency exhibits a broad maximum and remains high, while it drops quickly for DOTAP. This again demonstrates the importance of the membrane charge density for transfection with  $L_{\alpha}^c$  complexes as described in the preceding section [38].

## **FUTURE DIRECTIONS**

Thus far we have considered CL-DNA complexes whose interactions with cells are non-specific and typically mediated by electrostatic forces. In this section we describe ongoing experiments where directed interactions (i.e. ligand-receptor type) are added to CL-DNA complexes by incorporating peptide-lipids with specific amino-acid sequences. We have recently synthesized such lipids, which contain peptides on hydrophilic poly(ethylene glycol) (PEG) spacers of varied length. The general structure of the peptide-lipids is shown in Fig. (16) and examples of employed peptide ligands and spacers are given in Table 3. We are pursuing two major directions in this research effort. One are CL-DNA complexes that will target the nucleus via a nuclear localization

sequence. The other are complexes suitable for future systemic or in vivo studies, which will target cell surface receptors [27].

Insert Fig. 16

Insert Table 3.

**Surface Functionalized CL-DNA Complexes containing NLS Peptide-Lipids: CL-DNA Complexes for Transfecting Non-Dividing Cells.** A major continuing focus of work in our laboratory, and indeed for a large number of other laboratories worldwide working on non-viral gene delivery systems, is on optimizing transfection at the cell level in continuous (dividing) cell lines with potential relevance for the development of cancer vaccines [1,2,3,4,5,6,7]. Indeed, a large fraction of clinical work using CLs for delivery is centered around CL-DNA vaccines intended to induce transient expression of genes encoding for immuno-stimulatory proteins in dividing cells. The nuclear membrane, which dissolves during mitosis, is not a barrier in these experiments.

However, even cancer cells are dividing much more slowly than the cells used for in vitro experiments and some very interesting target cells for gene delivery, such as nerve cells, are non-dividing cells. Thus, vectors that are able to overcome the barrier posed by the nuclear membrane are of great interest. In the case of lamellar complexes, confocal microscopy shows that while released DNA is only at high membrane charge density, intact complex particles are present in the cell for both high and low membrane charge density. (Fig. (5 (B)) and Fig. (9)). In addition, our proposed mechanism entails the release of a smaller complex particle into the cytoplasm after fusion with the endosomal membrane. Thus, intracellular targeting of a fraction of the complexes via

peptide lipids should be feasible. We are investigating whether peptide-lipids containing the NLS of the SV 40 virus [46] can mediate transport of the fraction of CL-DNA complexes with a particle size of less than 25 nanometers through the nuclear pore. Colloidal particles of up to 25 nm diameter, when coated with SV 40 NLS peptide-conjugated bovine serum albumin (BSA), are transported into the nuclei of HeLa cells [47,48]. While dynamic light scattering data gives a typical average CL-DNA complex size of around 100 to 150 nm, the distribution of sizes is very broad, extending down to 10s of nanometers [4,14,15]. The larger particles observed in microscopy are likely aggregates of smaller particles. Furthermore, cryo electron microscopy data has shown that a fraction of complexes consists of as little as 2 to 3 lipid-bilayers complexed with DNA [49]. Optimizing TE for complexes that can cross the nuclear membrane is important for future delivery applications in slowly or non-dividing cells. Once inside the nucleus, the DNA will rapidly associate with histones or polyamines. We have observed both these processes in vitro (H. M. Evans, C. R. Safinya, unpublished and [21]).

**Surface-functionalized CL-DNA complexes containing RGD-based peptide-lipids: CL-DNA complexes for in vivo applications.** The attachment of CL-DNA complexes to mammalian cells and the resulting interactions (cf. Fig. (10), label a) are mediated through electrostatic attractions between cationic CL-DNA complexes and negatively charged cell surface sulfated proteoglycans [39]. We are investigating an RGD-peptide with the sequence GRGDSP, attached to a lipid to investigate alternative pathways of cell adhesion. The RGD sequence is expected to bind with high-affinity to the cell's surface integrins (i.e.  $\alpha_v\beta_3$  and  $\alpha_5\beta_1$ ), leading to receptor-mediated endocytosis. A main motivation for these experiments is that the concept could later be extended to

more specific ligands with the aim of targeting specific cell types for systemic in vivo applications.

Insert Fig. 17

CL-DNA complexes, as they are currently used in ex vivo and in vivo clinical trials, the latter involving intra-tumoral injection methods [1,2], are not suitable for systemic in vivo applications. Cationic lipids and their complexes with DNA activate the complement system [50], resulting in their rapid removal from circulation by the mononuclear phagocytic system cells through the process of opsonization. PEG-conjugation to poly(L-lysine) can reduce the activation of the complement system [50], a phenomenon well known for liposomes [51,52]. The presence of a hydrophilic polymeric shell on liposomes provides a repulsive barrier and results in vastly increased circulation lifetimes, which is referred to as steric stabilization. Thus, complexes designed for systemic delivery should contain a PEG coating to prevent opsonization. However, once the PEG layer is thick enough to effectively minimize undesired interactions, the complex will also no longer attach to cells and attachment through a specific ligand (with RGD serving as a model system) will be needed. The feasibility of this concept has been demonstrated for liposomes with antibodies as targeting moieties [53].

We have performed a series of transfection and XRD experiments using PEG-lipids of various lengths. We refer to these as PEG<sub>MW</sub>-lipids, where MW is the molecular weight of the PEG chain. Recent x-ray data show that CL-DNA complexes containing PEG<sub>2000</sub>-lipid, shown schematically in the top part of Fig. (17), are indeed structurally

stable and thus suitable candidates for the incorporation of additional RGD-PEG-lipids [54]. To demonstrate that the PEG<sub>2000</sub>-lipid is also exposed at the complex surface, we conducted TE measurements of highly transfecting CL-DNA complexes (80 mole% DOTAP) as a function of increasing amount of incorporated PEG-lipid (Fig. (17), bottom). The addition of about 6 mol-% PEG<sub>2000</sub>-lipid already leads to a strong suppression of TE, by about 2 orders of magnitude. This indicates that the electrostatic binding of the cationic CL-DNA complex to cells is efficiently reduced due to the PEG<sub>2000</sub> polymer coat of thickness  $\approx 35 \text{ \AA}$  [31]. In contrast, the shorter PEG chain of a PEG<sub>400</sub>-lipid does not provide significant shielding of the electrostatic interactions and TE remains relatively high. Note the difference in mol-fraction for the PEG-lipids, which correspond to approximately equal total amounts of PEG.

We are now investigating surface-functionalized CL-DNA complexes, which incorporate a mixture of PEG<sub>2000</sub>-lipids and RGD-PEG<sub>2000</sub>-lipids within their membranes. The RGD-peptide should provide an effective ligand for the integrin receptors on the cell surface. For such functionalized CL-DNA complexes, the primary role of the cationic lipid is the condensation of DNA. This is in contrast to standard CL-DNA complexes, where the cationic lipids both condense DNA and provide for electrostatic attachment to the cell surface. Therefore, the new complexes are not only designed to be suitable for systemic in vivo applications due to their steric stabilization, but the reduced amount of cationic lipid will also reduce their toxicity.

## CONCLUSIONS

The broad, long-term objective of our research is to develop a fundamental science base, which will lead to the design and synthesis of optimal nonviral carriers of DNA for

gene therapy. Simultaneously, a major long term objective is to improve efficiency for delivering large pieces of DNA containing important human genes and their regulatory sequences (> 100 k-base-pairs), which at present can only be achieved with synthetic vectors. The structure-function data obtained from our research should allow us to begin the formidable task of rationally designing these self assemblies for enhanced gene delivery, beginning with the chemical structure of the lipids and the appropriate lipid compositions.

Our work has shown that CL-DNA complexes of distinct structure (i.e.  $L_{\alpha}^c$  versus  $H_{II}^c$ ) differ widely in their interactions with cells and their ability to deliver exogenous DNA to the cytoplasm. We have demonstrated that  $\sigma_M$ , the average membrane charge density of the CL-vector, is a key universal parameter that governs the transfection behavior of  $L_{\alpha}^c$  complexes in cells. The universal TE curve for DOPC-containing  $L_{\alpha}^c$  complexes increases exponentially with  $\sigma_M$  for  $\sigma_M < \sigma_M^*$  (an optimal membrane charge density), and saturates for  $\sigma_M > \sigma_M^*$ . The limiting saturated TE level of  $L_{\alpha}^c$  complexes is comparable to the high TE of DOPE-containing  $H_{II}^c$  complexes, which exhibit no dependence on  $\sigma_M$ . For both  $L_{\alpha}^c$  and  $H_{II}^c$  complexes, confocal microscopy reveals that much of the lipid-released DNA is in a condensed state and therefore has to contain oppositely charged macro-ion condensing agents from the cytoplasm. While DNA strands covering the surface of the DNA mass or isolated from it are most likely transcriptionally active, much of the observed bulk of condensed DNA may be transcriptionally inactive, probably setting the current limit to transfection by cationic lipid vectors. Future studies should reveal well-defined structure-function correlations for transfection in vivo, in particular, for local intra-tumoral injection in clinical studies.

## **ACKNOWLEDGEMENTS**

We gratefully acknowledge the contributions of recent collaborators, in particular, Joachim Rädler, Ilya Koltover, Cyril George, Tim Salditt, Uwe Schulze, and Hans-Werner Schmidt. We have benefited over the years through extensive discussions with Phillip Felgner, Leaf Huang, Robijn Bruinsma, Tom Lubensky, Philip Pincus, Bill Gelbart, and Avinoam Ben-Shaul. The work was supported by grant GM-59288 from the National Institute of General Medical Sciences of the National Institute of Health on DNA-lipid gene delivery studies. Support was also provided by the National Science Foundation DMR 0203755, and National Institute of Health grants AI-20611 and AI-12520. DOSPA and DMRIE were gifts from Phillip Felgner for which we are grateful. The synchrotron x-ray diffraction experiments were carried out at the Stanford Synchrotron Radiation Laboratory, which is supported by the U.S. Department of Energy. The Materials Research Laboratory at UC Santa Barbara is supported by NSF-DMR-0080034.



## Tables

Table 1. Open gene therapy clinical trials worldwide as of May 2003.

---

	Number of open clinical trials worldwide	Diseases treated
<b><u>Viral Vectors</u></b>		
Retrovirus	161	Cancers, SCID, AIDS, hemophilia, others
Adenovirus	135	Cancers, cystic fibrosis, peripheral artery disease, others
Pox virus	37	Cancers
Adeno-associated virus	9	Cystic fibrosis, hemophilia, prostate cancer
Other viral	6	Cancers
<b><u>Nonviral Vectors</u></b>		
Lipofection	57	Cancers, cystic fibrosis, coronary artery disease, restenosis
Naked DNA	59	Cancers, artery diseases, others
RNA transfer	6	Cancers
Gene gun	4	Skin cancers

---

Table 2. Newly synthesized multivalent cationic lipids. A spacer n of 2, 8, 22 and 43 corresponds to a PEG molecular weight of 150, 400, 1000 and 2000, respectively.

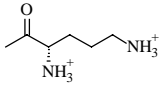
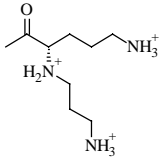
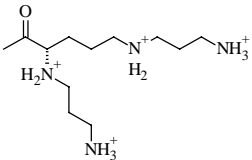
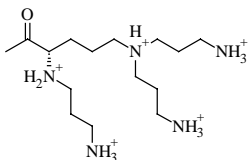
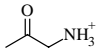
Head group	Spacer (EO)n	Maximum head group charge	Lipid name
	0 2, 8, 22, 43 (ester linkage)	+2	MVL2
	0	+3	MVL3
	0	+4	MVL4
	0, 2	+5	MVL5 / TMVL5 (n=2)
	0	+1	MVL1

Table 3. Compilation of recently synthesized peptide-lipids.

Peptide Sequence	Spacer
GPKKKRKV (SV 40 NLS)	PEG 400 (n =9) PEG 1000 (n=23)
GRGDSP	PEG 2000 (n = 43)

## Figure Captions

Fig. 1

Schematic of CL-DNA complex formation: **(A)**: Cationic liposomes, closed spherical shells of bilayers consisting of cationic and neutral lipids; **(B)**: DNA, with cationic counterions condensed on the backbone. Scale bar for (A) only. Entropy gain from release of tightly bound counterions **(C)** is the main driving force for complex formation. **(D)** A typical optical micrograph (differential interference contrast mode) of CL-DNA-complexes.

Fig. 2

Mixing of DNA and CLs results in the spontaneous formation of CL-DNA complexes with well-defined self-assembled structures. The schematic on the left shows the local structure of their interior on the nanometer scale for the most commonly observed lamellar phase (denoted  $L_{\alpha}^c$ ). As derived from synchrotron x-ray diffraction data, the structure consists of alternating lipid bilayers DNA monolayers. The interlayer spacing is  $d = \delta_w + \delta_m$ . For certain lipids, mixing of DNA and CLs results in the spontaneous formation of a different self-assembled structure (denoted  $H_{II}^c$ ) of CL-DNA complexes, as shown on the right. The internal structure of the inverted hexagonal  $H_{II}^c$  phase of CL-DNA complexes is comprised of DNA coated with a lipid monolayer arranged on a hexagonal lattice, as derived from synchrotron x-ray diffraction data. Neutral and cationic lipids are depicted as having white and gray headgroups, respectively. Adapted from [14,15].

Fig. 3

Chemical structures of cationic and neutral lipids with their abbreviated names.

Fig. 4

Comparison of CL-DNA complex structure and transfection efficiency. Complexes were prepared using pGL3 plasmid DNA. **Left:** Small angle x-ray scattering pattern and schematic view (inset) of lamellar  $L_{\alpha}^c$  complexes (mole fraction  $\Phi_{\text{DOPC}} = 0.67$ ). **Right:** Small angle x-ray scattering pattern and schematic view (inset) of inverted hexagonal (inset)  $H_{II}^c$  complexes (mole fraction  $\Phi_{\text{DOPE}} = 0.69$ ). **Middle:** TE of the complexes, as measured by luciferase enzyme assays of transfected mouse L cells. Adapted from [38].

Fig. 5

Laser scanning confocal microscopy images of transfected mouse L cells fixed six hours after incubation with complexes. Red and green fluorescence corresponds to lipid and DNA labels, respectively; yellow, the overlap of the two, denotes CL-DNA complexes. For each set, middle is the x-y (top) view at a given z; right is the y-z side view along the vertical dotted line; bottom is the x-z side view along the horizontal dotted line. Arrows in the x-z and y-z plane side views indicate objects in circles. **(A):** Cells transfected with  $H_{II}^c$  complexes ( $\Phi_{\text{DOPE}} = 0.69$ ), show fusion of lipid with the cell plasma membrane and the release of DNA (green in the circle) within the cell. Thus,  $H_{II}^c$  complexes display clear evidence of separation of lipid and DNA, which is consistent with the high transfection efficiency of such complexes. Very significantly, the observed DNA is in an aggregated state, which implies that it resides in the cytoplasm and has escaped the endosome. **(B):**

Cells transfected with  $L_{\alpha}^c$  complexes at  $\Phi_{\text{DOPC}} = 0.67$  which results in a low membrane charge density  $\sigma_M \cdot 0.005 \text{ e}/\text{\AA}^2$  and low transfection efficiency as shown in Fig. (4). No fusion is visible and intact CL-DNA complexes such as the one marked with the circle are observed inside the cells. The observation of intact complexes implies that DNA remains trapped within the complexes, which is consistent with the observed low transfection efficiency. The cell outline was observed in reflection mode and therefore appears as blue. Bars = 5  $\mu\text{m}$  for all planes. Adapted from [38].

Fig. 6

(A) Transfection efficiency as RLU per mg total cellular protein, plotted as a function of varying mole fraction DOPC with cationic lipids DOSPA, DOTAP, and DMRIE. (B) TE plotted versus the membrane charge density  $\sigma_M$ , demonstrating universal behavior of complexes containing cationic lipids with different charge and head group area (inset). For all three systems, TE increases with  $\sigma_M$  until an optimal  $\sigma_M^*$  (arrow at  $\cdot 0.0104 \text{ e}/\text{\AA}^2$ ; determined by the intersection of two straight lines fit to the data (dashed lines) above and below the “knee”), at which TE plateaus. Adapted from [38].

Fig. 7

The fractional TE increase  $\text{TE}_{\text{chloroquine}}/\text{TE}$  for the DOSPA/DOPC and DOTAP/DOPC systems with added chloroquine as a function of  $\sigma_M$ . Note the logarithmic scale. The fractional increase is substantial for low membrane charge densities, indicating that endosomal escape is limiting in this regime. Adapted from [38].

Fig. 8

TE plotted as a function of mole fraction of neutral lipid for the DOTAP/DOPC and the DOTAP/DOPE systems. DOTAP/DOPC-DNA complexes exhibit the  $L_{\alpha}^c$  phase. As described in the text, the same amount of total charged species was used for each TE data point (which are spread out over nearly four decades) and the membrane charge density of CL-DNA complexes ( $\sigma_M$ ) was varied solely by changing the amount of neutral lipid.

Adapted from [38].

Fig. 9

Typical LSCM images of a mouse L cell transfected with  $L_{\alpha}^c$  complexes at  $\Phi_{\text{DOPC}} = 0.18$ , corresponding to cationic membranes with a high charge density  $\sigma_M \cdot 0.012 \text{ e}/\text{\AA}^2$  and high transfection efficiency (cf. Fig. (6)). Red and green fluorescence corresponds to lipid and DNA labels, respectively; yellow, the overlap of the two, denotes CL-DNA complexes.

**Top:** The left image is an x-y (top) view at a given z. Arrows in the side views indicate objects in circles in the x-y plane. The panels on the right are y-z side views along the vertical dashed lines in the x-y plane. **Bottom:** The panels on the left are x-z side views along the horizontal dashed lines in the x-y plane. In the boxes on the right, plots of lipid and DNA fluorescence intensity along the x-y diagonal or z-axis are shown. Although the lamellar complexes used here show similarly high TE, no lipid transfer to the cell plasma membrane is seen in contrast to high-transfecting  $H_{II}^c$  complexes (Fig. (5 (A))). Both released DNA (circle “1”) and intact complexes (circle “2”) are observed inside the cell. Labels (3) and (4): A complex in the process of releasing its DNA into the cytoplasm. Corresponding plots of fluorescence intensity as a function of position are

shown in boxes in the lower right corner. The cell outline was observed in reflection mode and therefore appears as blue. Bars = 5  $\mu\text{m}$  for all planes. Adapted from [38].

Fig. 10

Model of cellular uptake of  $L_{\alpha}^c$  complexes. **(a)** Cationic complexes adhere to cells due to electrostatic attraction between positively charged CL-DNA complexes and negatively charged cell-surface sulfated proteoglycans (shown in expanded views) of mammalian plasma membranes. **(b and c)** After attachment, complexes enter through endocytosis. **(d)** Only those complexes with a large enough membrane charge density ( $\sigma_M$ ) escape the endosome through activated fusion with endosomal membranes. **(e)** Released DNA inside the cell is observed by confocal microscopy to be present primarily in the form of aggregates. The DNA aggregates must reside in the cytoplasm because oppositely charged cellular biomolecules able to condense DNA are not present in the endosome. Arrows in the expanded view of (c) indicate the electrostatic attraction between the oppositely charged membranes of the complex and endosome, which tends to enhance adhesion and fusion. Arrows in the expanded view of (d) indicate the bending of the membranes required for fusion, which constitutes the main barrier for the process.

Adapted from [38].

Fig. 11

Schematic sketch of an inverted hexagonal CL-DNA complex interacting with either the plasma membrane or the endosomal membrane (a). The cell-surface proteoglycans of the cellular membrane (cf. Fig. (10)) have been omitted for clarity. The outer lipid



monolayer covering the  $H_{II}^C$  CL-DNA complex has a positive curvature, whereas the preferred curvature of the cationic lipids is negative as realized in the monolayers coating DNA within the complex. Thus, the outer layer is energetically costly, which results in a driving force, independent of the cationic membrane charge density, for rapid fusion of the  $H_{II}^C$  complex with the bilayer of the cell plasma membrane or the endosomal membrane as sketched in (b). Adapted from [38].

Fig. 12

General structure of ornithine-based multivalent lipids.

Fig. 13

Optical microscopy images of CL-DNA complexes prepared from DOPC, MVL5 and plasmid DNA in differential-interference-contrast mode (left), DNA fluorescence (middle, YOYO green) and lipid fluorescence (right, DHPE-Texas Red). Adapted from [24].

Fig. 14

Small angle XRD patterns of CL-DNA complexes in DMEM for DOTAP/DOPC (top) and MVL5/DOPC (bottom) lipid mixtures at similar cationic to neutral lipid molar ratios (31:69 for MVL5; 33:67 for DOTAP). The complexes are in the lamellar  $L_{\alpha}^C$ -phase. At the same molar ratio of cationic to neutral lipid, the DNA interaxial spacing is reduced from 59 Å to 31 Å in the complexes with MVL5, reflecting the higher membrane charge density. Adapted from [24].

Fig. 15

Transfection efficiencies in mouse L cells for cationic lipids DOTAP and MVL5 in mixtures with DOPC. Adapted from [24].

Fig. 16

General structure of the peptide-lipids. The spacer moiety consists of PEG of variable length.

Fig. 17

**Top:** Schematic of a cross-section of a CL-DNA complex containing PEG-Lipids. Gray circles represent the DNA rods. **Bottom:** Transfection efficiency of PEG-lipid/DOTAP/DOPC-DNA complexes ( $\Phi_{\text{DOTAP}} = 0.8$ ) as a function of increasing content of PEG-lipid. The PEG<sub>2000</sub>-lipid blocks the electrostatic binding of complexes to cells, whereas the PEG<sub>400</sub>-lipid has a much weaker effect due to its shorter chain length. Note the difference in mol-fraction for the PEG-lipids, which correspond to approximately equal total amounts of PEG.

## Figures

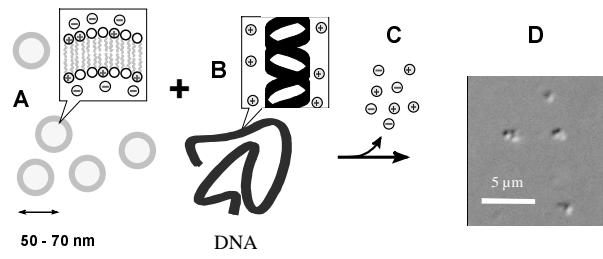


**Figure 1**

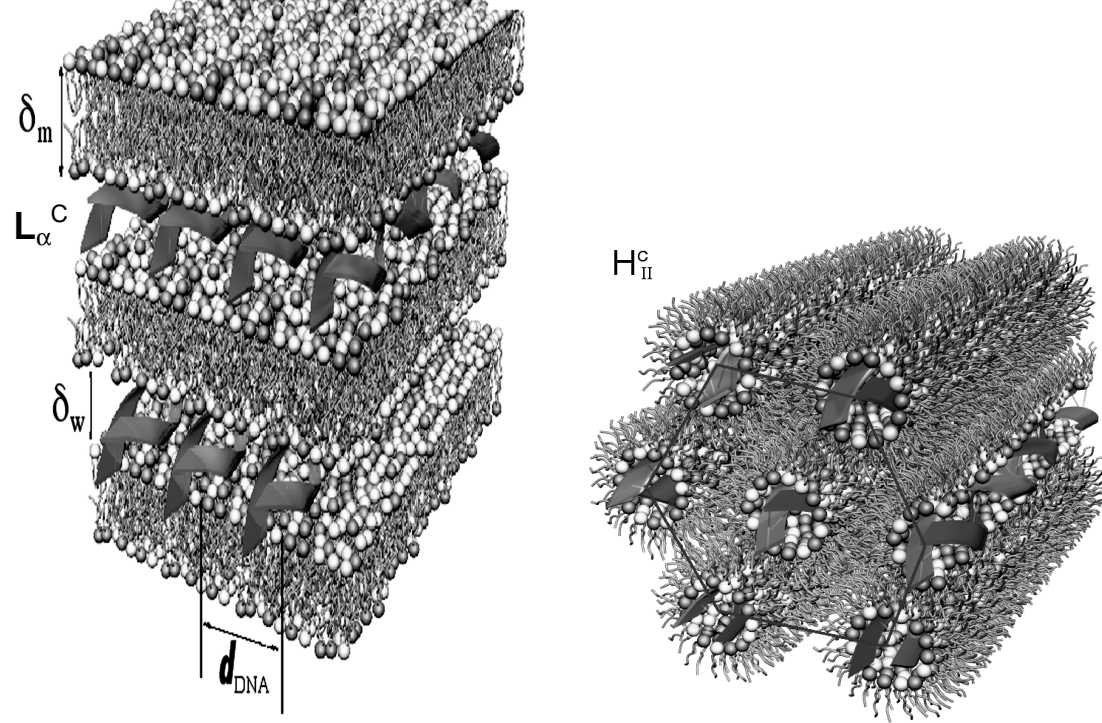


**Figure 2**

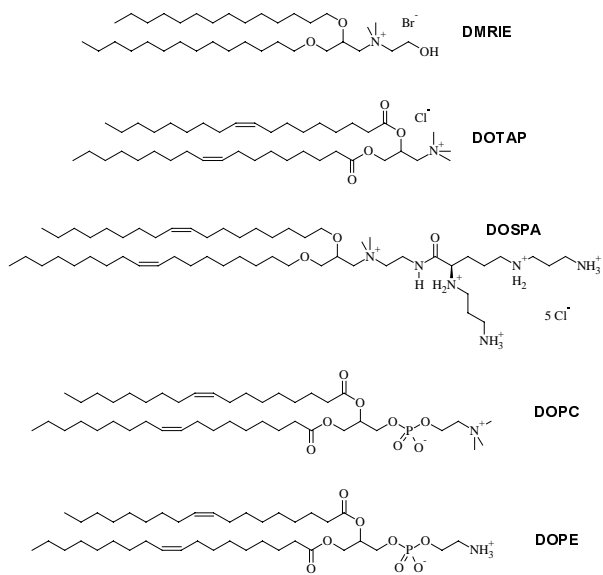


**Figure 3**

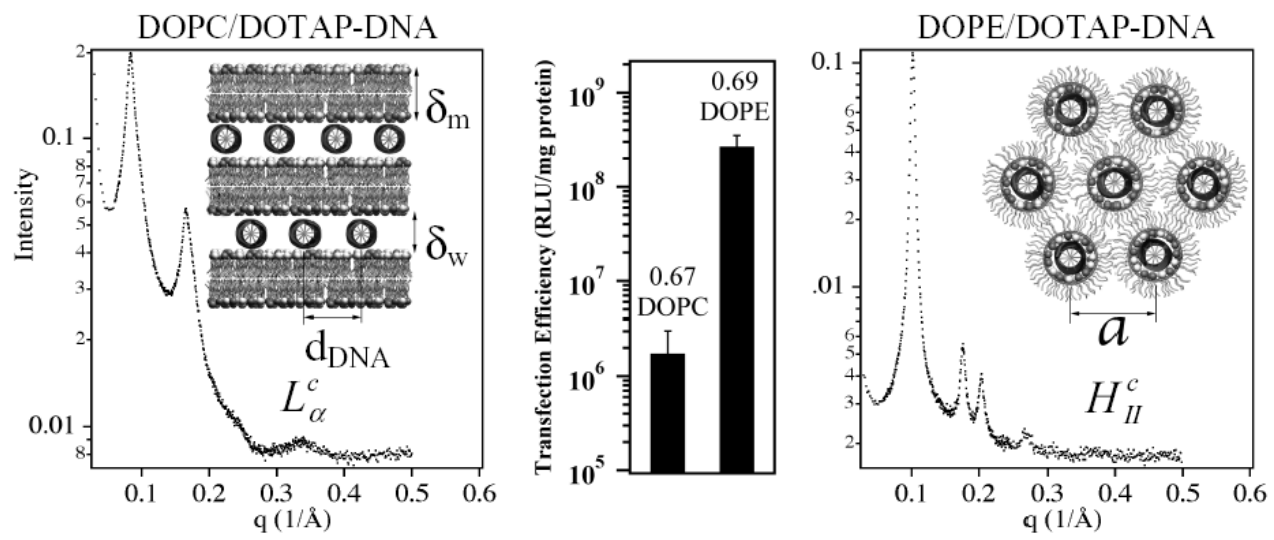


**Figure 4**

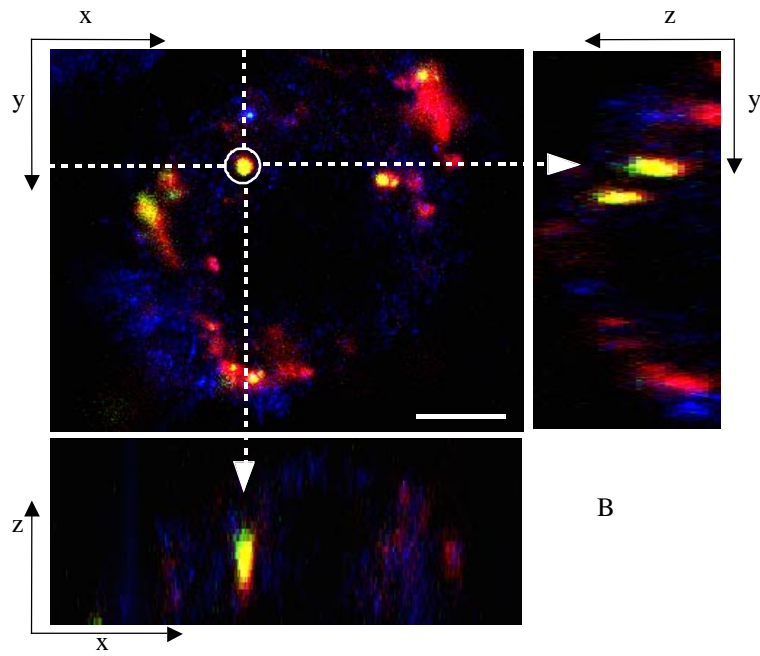
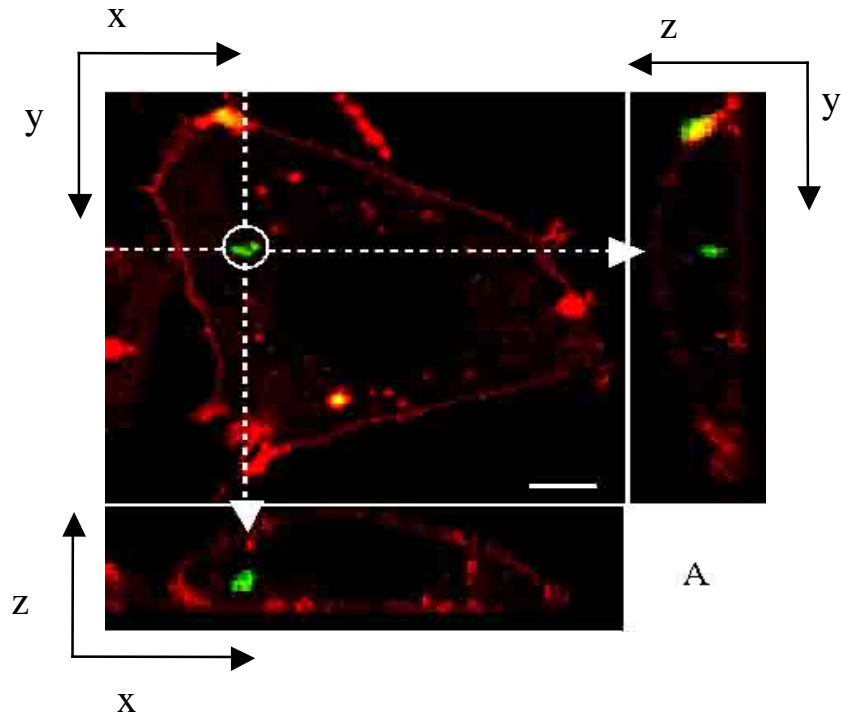


**Figure 5**

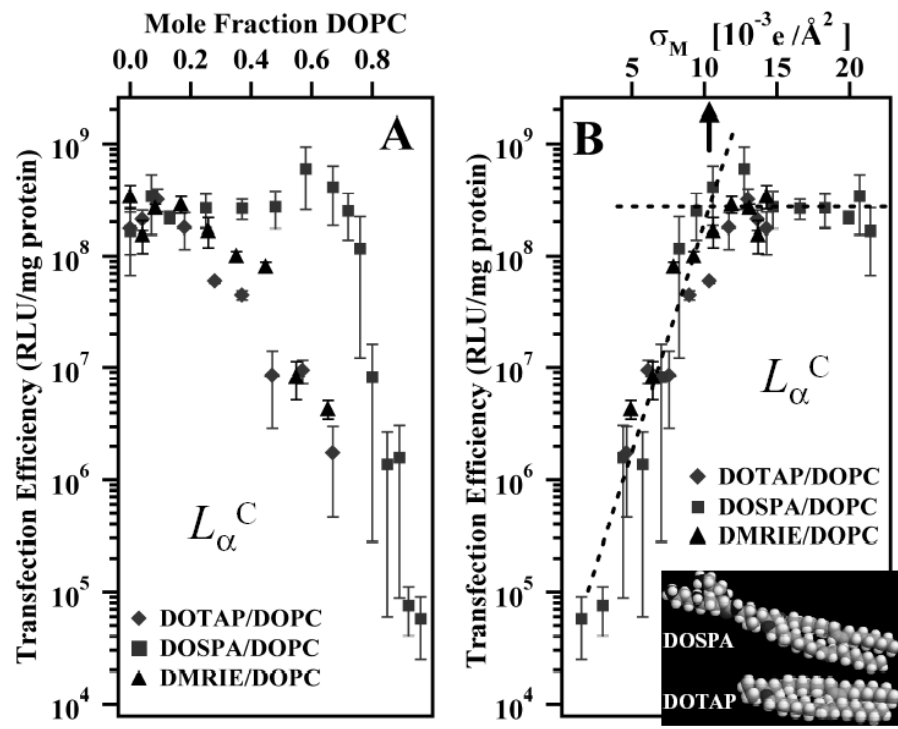


**Figure 6**



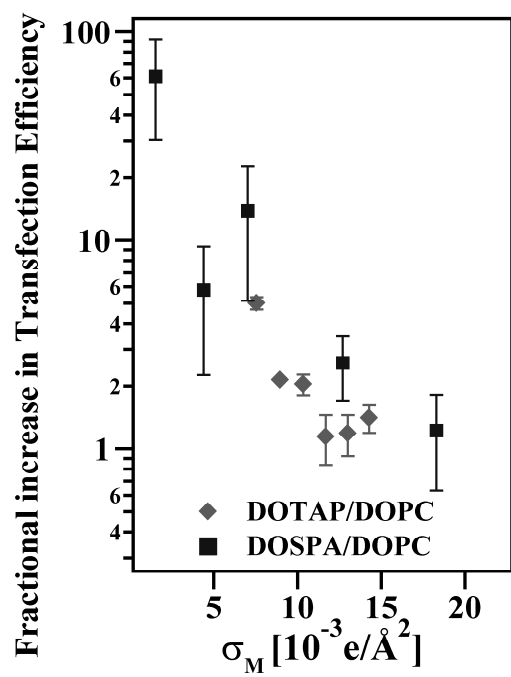


**Figure 7**

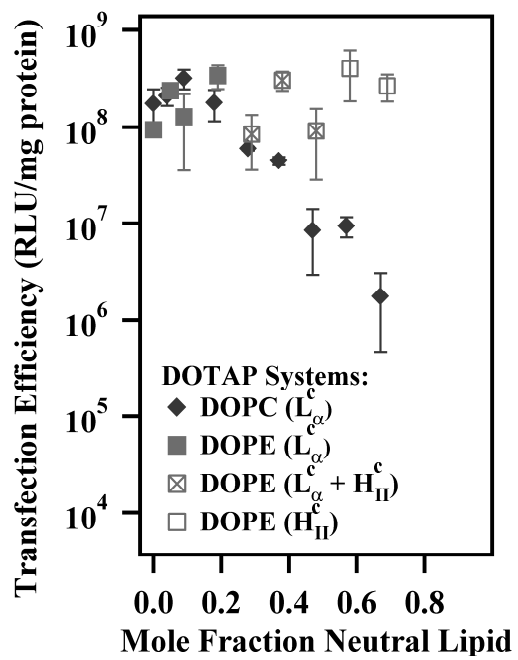


**Figure 8**

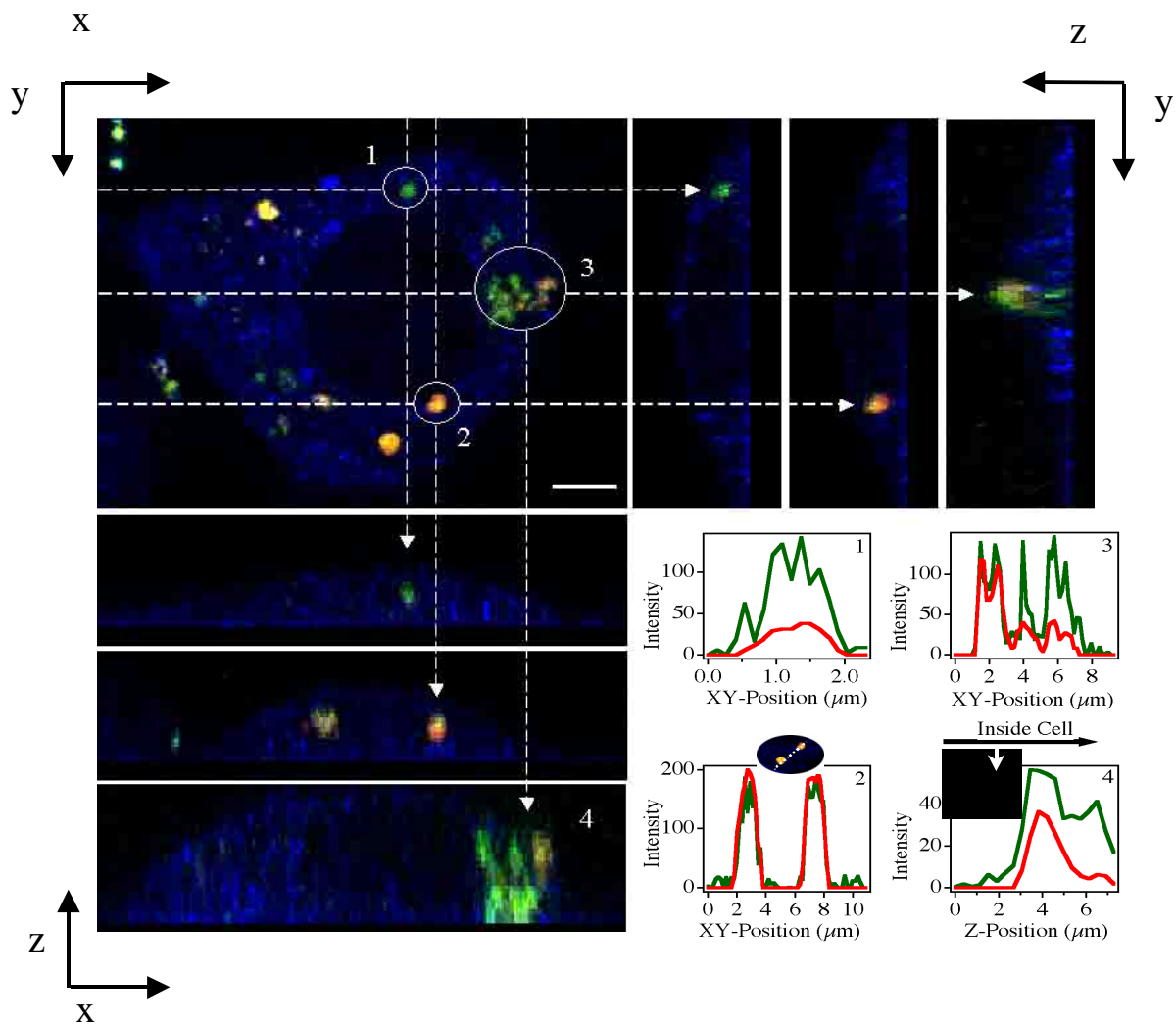
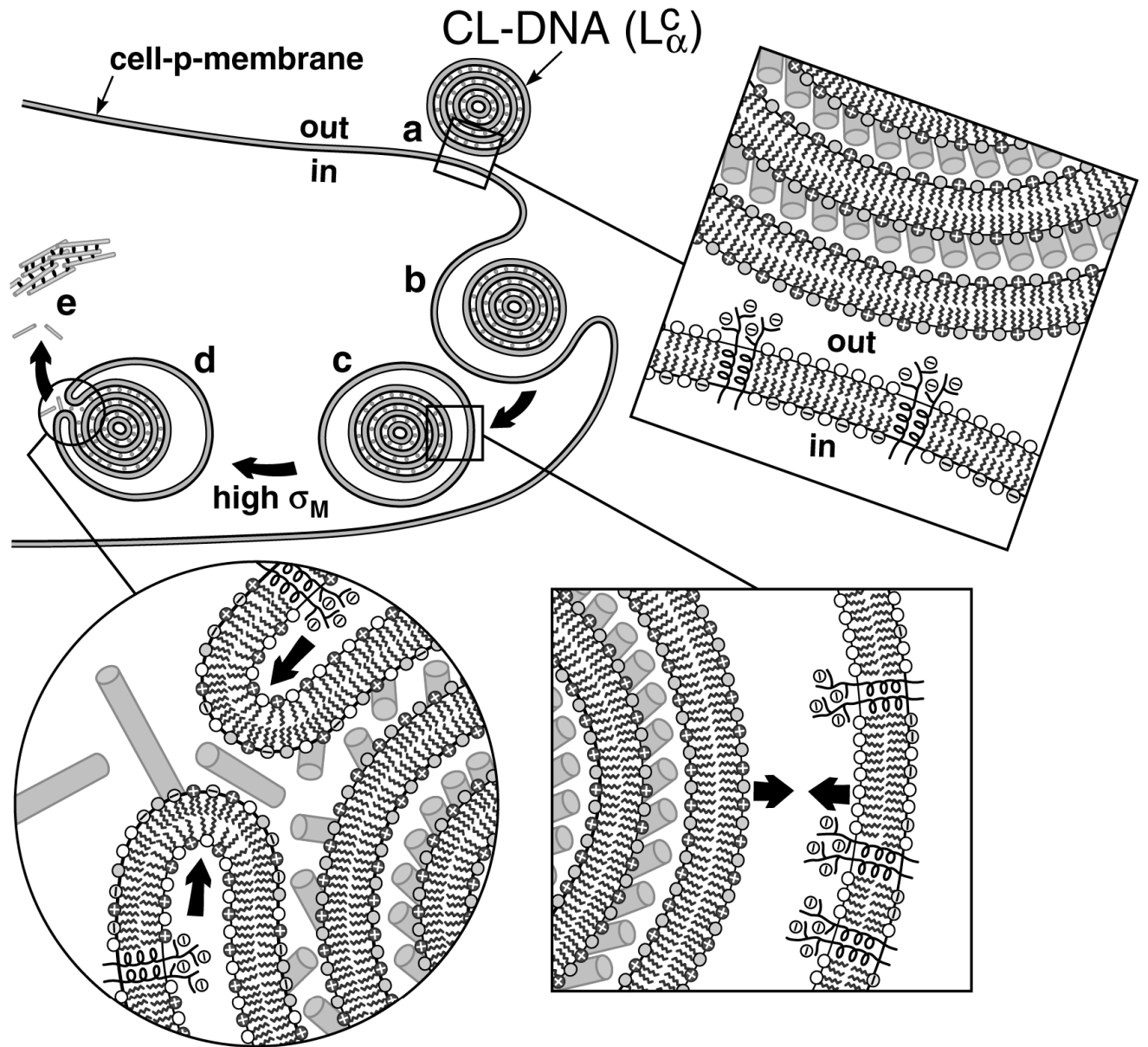
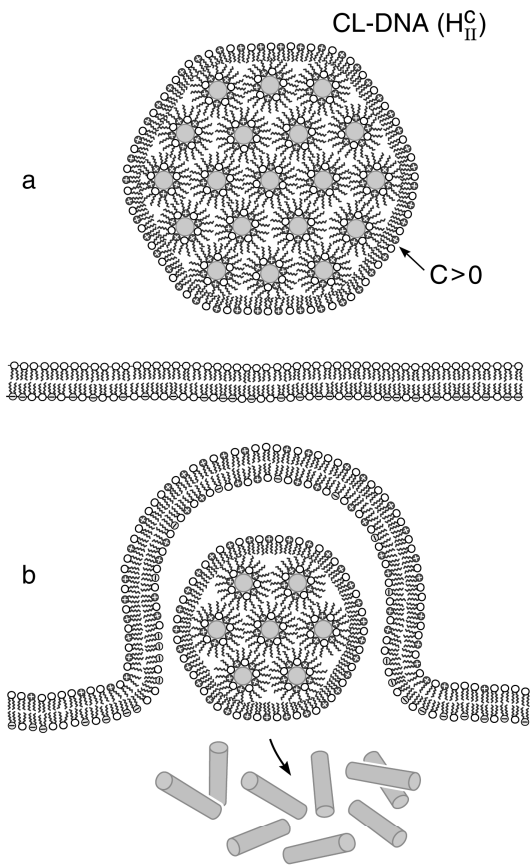


Figure 9



**Figure 10**



**Figure 11**

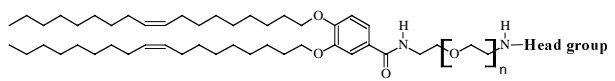


**Figure 12**

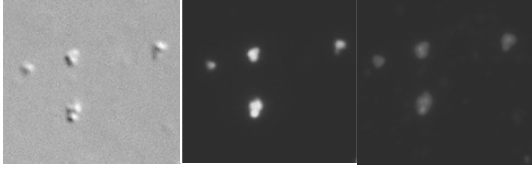


**Figure 13**

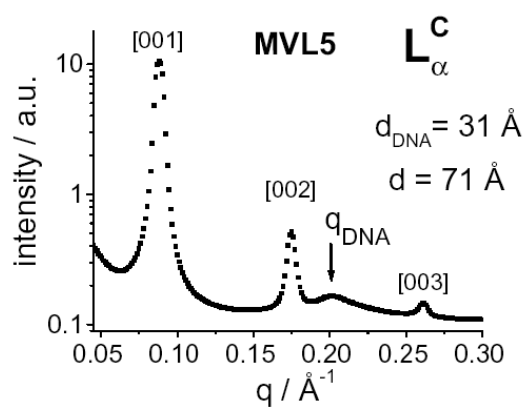
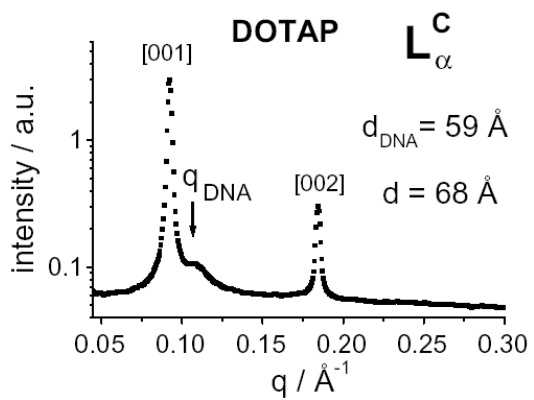


**Figure 14**



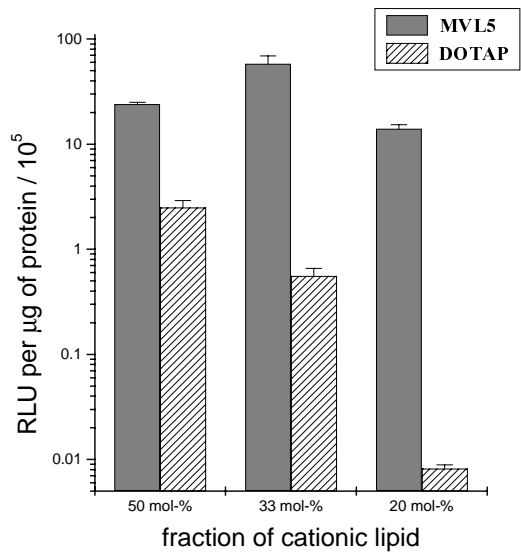


**Figure 15**

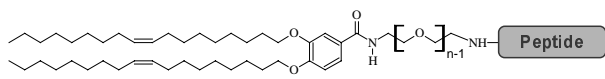


**Figure 16**

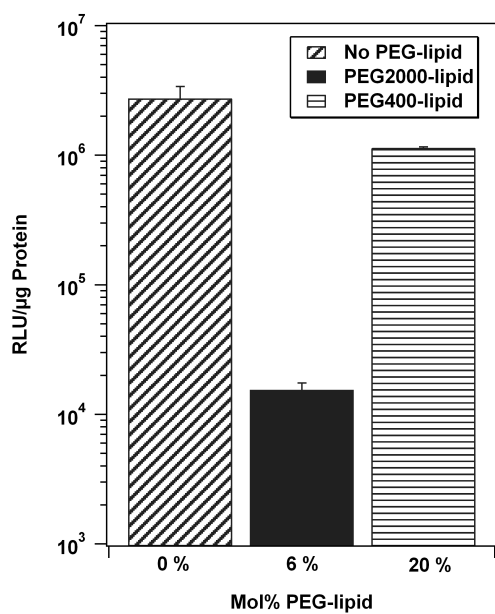
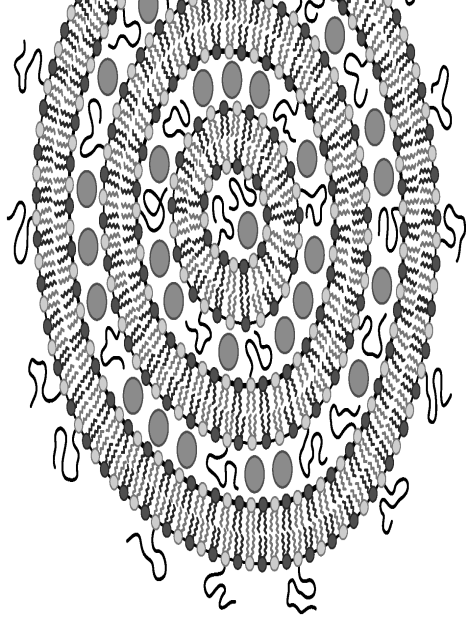


**Figure 17**

## REFERENCES

- <sup>1</sup> Henry, C.M. *Chem. Eng. News*, **2001**, 79(48), 35.
- <sup>2</sup> Ferber, D. *Science*, **2001**, 294, 1638.
- <sup>3</sup> Alper, J. *Science*, **2002**, 296, 838.
- <sup>4</sup> Chesnoy, S.; Huang, L. *Annu. Rev. Biophys. Biomol. Struct.*, **2000**, 29, 27.
- <sup>5</sup> Friedmann, T. *Sci. Am.*, **1997**, 276, 96.
- <sup>6</sup> Clark, P.R.; Hersh, E.M. *Curr. Opin. Mol. Ther.*, **1999**, 1, 158.
- <sup>7</sup> Miller, A. D. *Angew. Chem., Int. Ed.*, **1998**, 37, 1768.
- <sup>8</sup> Felgner, P.L.; Gadek, T.R.; Holm, M.; Roman, R.; Chan, H.W.; Wenz, M.; Northrop, J.P.; Ringold, G. M.; Danielsen, M. *Proc. Natl. Acad. Sci. U.S.A.*, **1987**, 84, 7413.
- <sup>9</sup> Wolff, J. A. Ed. *Gene Therapeutics: Methods and Applications of Direct Gene Transfer*, Birkhäuser, Boston, **1994**.
- <sup>10</sup> Nabel, G.; Nabel, E.; Yang, Z.; Fox, B.; Plautz, G.; Gao, X.; Huang, L.; Shu, S.; Gordon, D.; Chang, A. *Proc. Natl. Acad. Sci. U.S.A.*, **1993**, 90, 11307.
- <sup>11</sup> Extensive and current information on clinical trials in the field of gene therapy can be found on the internet at <http://www.wiley.co.uk/genetherapy/clinical/>.
- <sup>12</sup> Marshall, E. *Science*, **2000**, 288, 951.
- <sup>13</sup> Marshall, E. *Science*, **2002**, 298, 510.
- <sup>14</sup> Rädler, J.O.; Koltover, I.; Salditt, T.; Safinya, C.R. *Science*, **1997**, 275, 810.
- <sup>15</sup> Koltover, I.; Salditt, T.; Rädler, J.O.; Safinya, C.R. *Science*, **1998**, 281, 78.
- <sup>16</sup> Lasic, D.D.; Strey, H.; Stuart, M.C.A.; Podgornik, R.; Frederik, P.M. *J. Am. Chem. Soc.*, **1997**, 119, 832.

- <sup>17</sup> Harrington, J.J.; van Bokkelen, G.; Mays, R.W.; Gustashaw, K.; Williard, H.F. *Nat. Genet.*, **1997**, *15*, 345.
- <sup>18</sup> Willard, H.F. *Science*, **2000**, *290*, 1308.
- <sup>19</sup> Koltover, I.; Salditt, T.; Safinya, C.R. *Biophys. J.*, **1999**, *77*, 915.
- <sup>20</sup> Salditt, T.; Koltover, I.; Rädler, J.O.; Safinya, C.R. *Phys. Rev. Lett.*, **1997**, *79*, 2582.
- <sup>21</sup> Koltover, I.; Wagner, K.; Safinya, C.R. *Proc. Natl. Acad. Sci. U.S.A.*, **2000**, *97*, 14046.
- <sup>22</sup> Safinya, C.R. *Curr. Opin. Struc. Biol.*, **2001**, *11*, 440.
- <sup>23</sup> Schulze, U.; Schmidt, H.-W.; Safinya, C.R. *Bioconjugate Chem.*, **1999**, *10*, 548.
- <sup>24</sup> Ewert, K., Ahmad, A.; Evans, H.M.; Schmidt, H.-W.; Safinya, C.R. *J. Med. Chem.*, **2002**, *45*, 5023.
- <sup>25</sup> Rinehart, J.; Hersh, E.; Issell, B.; Triozzi, P.; Buhles, W.; Neidhart, J. *Cancer Invest.*, **1997**, *15*, 403.
- <sup>26</sup> Stopeck, A.T.; Hersh, E.M.; Brailey, J.L.; Clark, P.R.; Norman, J.; Parker, S.E. *Cancer Gene Ther.*, **1998**, *5*, 119.
- <sup>27</sup> Ewert, K.; Safinya, C. R. manuscript in preparation.
- <sup>28</sup> Farhood, H.; Serbina, N.; Huang, L. *Biochim. Biophys. Acta*, **1995**, *1235*, 289.
- <sup>29</sup> Hui, S.; Langner, M.; Zhao, Y.; Ross, P.; Hurley, E.; Chan, K. *Biophys. J.*, **1996**, *71*, 590.
- <sup>30</sup> Lin, A.J.; Slack, N.L.; Ahmad, A.; Koltover, I.; George, C.X.; Samuel, C.E.; Safinya, C.R. *J. Drug Targeting*, **2000**, *8*, 13.
- <sup>31</sup> Wrobel, I.; Collins, D. *Biochim. Biophys. Acta*, **1995**, *1235*, 296.
- <sup>32</sup> Zabner, J.; Fasbender, A.J.; Moninger, T.; Poellinger, K.A.; Welsh, M.A. *J. Biol. Chem.*, **1995**, *270*, 18997.

- <sup>33</sup> Xu, Y.H.; Szoka, F.C. *Biochemistry*, **1996**, *35*, 5616.
- <sup>34</sup> Tristram-Nagle, S.; Petrache, H.I.; Nagle, J.F. *Biophys. J.*, **1998**, *75*, 917.
- <sup>35</sup> Felgner, P.L. *Adv. Drug Deliv. Rev.*, **1990**, *5*, 163.
- <sup>36</sup> Voet, D.; Voet, J. *Biochemistry*, Wiley, New York, **1995**.
- <sup>37</sup> Bloomfield, V.A. *Biopolymers*, **1991**, *31*, 1471.
- <sup>38</sup> Lin, A.J.; Slack, N.L.; Ahmad, A.; George, C.X.; Samuel, C.E.; Safinya, C.R. *Biophys. J.*, **2003**, *84*, 1.
- <sup>39</sup> Mislick, K.A.; Baldeschwieler, J.D. *Proc. Natl. Acad. Sci. U.S.A.*, **1996**, *93*, 12349.
- <sup>40</sup> Helfrich, W. *Z. Naturforsch.*, **1973**, *28c*, 693.
- <sup>41</sup> Seddon, J.M. *Biochim. Biophys. Acta*, **1990**, *1031*, 1.
- <sup>42</sup> Janiak, M.J.; Small, D.M.; Shipley, G.G. *J. Biol. Chem.*, **1979**, *254*, 6068.
- <sup>43</sup> Gompper, G.; Goos, J. *J. Phys. II (France)*, **1995**, *5*, 621.
- <sup>44</sup> Wong, G.C.L.; Tang, J.X.; Lin, A.; Li, Y.; Janmey, P.A.; Safinya, C.R. *Science*, **2000**, *288*, 2035.
- <sup>45</sup> Remy, J.-S.; Sirlin, C.; Vierling, P.; Behr, J.-P. *Bioconjugate Chem.*, **1994**, *5*, 647.
- <sup>46</sup> Kalderon, D.; Roberts, B.L.; Richardson, W.D.; Smith, A.E. *Cell*, **1984**, *39*, 499.
- <sup>47</sup> Dworetzky, S.I.; Lanford, R.E.; Feldherr, C.M. *J. Cell Biol.*, **1988**, *107*, 1279.
- <sup>48</sup> Feldherr C. M.; Akin, D. *J. Cell Biol.*, **1990**, *111*, 1.
- <sup>49</sup> Smyth Templeton, N.; Lasic, D.D.; Frederik, P.M.; Strey, H.H.; Roberts, D.D.; Pavlakis, G.N. *Nat. Biotechnol.*, **1997**, *15*, 647.
- <sup>50</sup> Plank, C.; Mechtler, K.; Szoka, F.C.; Wagner, E. *Human Gene Ther.* **1996**, *7*, 1437.
- <sup>51</sup> Bradley, A.J.; Devine, D.V.; Ansell, S.M.; Janzen, J.; Brooks, D.E. *Arch. Biochem. Biophys.*, **1998**, *357*, 185.

<sup>52</sup> Lasic, D.D.; Martin, F.J. Eds. *Stealth liposomes*, CRC Press, Boca Raton, **1995**.

<sup>53</sup> Allen T. M. *Trends Pharmacol. Sci.*, **1994**, *15*, 215.

<sup>54</sup> Martin-Herranz, A.; Ahmad, A.; Evans, H.M.; Ewert, K.; Schulze, U.; Schmidt, H.-W.; Safinya, C.R., submitted to *Biophys. J.*